doi.org/10.26434/chemrxiv.7636451.v1

Low Potential Prussian Blue Analogs: Manganese Hexacyanochromate

Samuel Wheeler, Isaac Capone, Sarah Day, Chiu C. Tang, Mauro Pasta

Submitted date: 27/01/2019 • Posted date: 28/01/2019

Citation information: Wheeler, Samuel; Capone, Isaac; Day, Sarah; Tang, Chiu C.; Pasta, Mauro (2019): Low Potential Prussian Blue Analogs: Manganese Hexacyanochromate. ChemRxiv. Preprint.

Prussian blue analogues (PBAs) have recently shown outstanding electrochemical properties ascribable to their unique open-framework crystal structure that allows the reversible insertion of alkali ions with negligible perturbation to the framework itself. Many hexacyanoferrate materials have shown excellent properties and are some of the most promising sodium- and potassium-ion cathode materials in both aqueous and organic electrolytes. However, there is a distinct lack of candidate PBA materials that operate at low potentials as their characteristic crystalline framework shows instability. In this article we characterise the structure and electrochemical behavior of manganese hexacyanochromate which exhibits reversible sodium insertion at -0.86 V vs. SHE (1.84 V vs. Na^+/Na), whilst maintaining the characteristic PBA cubic structure. This is the lowest redox potential of reported PBA materials and shows fast kinetics in a high voltage water-in-salt electrolyte. Further reduction in potential in an organic electrolyte shows decomposition of the crystalline structure.

File list (2)

Article.pdf (10.82 MiB)	view on ChemRxiv • download file
Article_SI.pdf (445.54 KiB)	view on ChemRxiv • download file

Low Potential Prussian Blue Analogs: Manganese Hexacyanochromate

Samuel Wheeler[1], Isaac Capone[1], Sarah Day[2], Chiu Tang[2], Mauro Pasta[1,*]

[1]Department of Materials, University of Oxford, Parks Road, Oxford OX1 3PH, United Kingdom

[2]I11 Beamline, Diamond Light Source Limited, Harwell Science and Innovation Campus, Chilton, Didcot OX11 0DE, United Kingdom

*Correspondence: mauro.pasta@materials.ox.ac.uk

Abstract

Prussian blue analogues (PBAs) have recently shown outstanding electrochemical properties ascribable to their unique open-framework crystal structure that allows the reversible insertion of alkali ions with negligible perturbation to the framework itself. Many hexacyanoferrate materials have shown excellent properties and are some of the most promising sodium- and potassium-ion cathode materials in both aqueous and organic electrolytes. However, there is a distinct lack of candidate PBA materials that operate at low potentials as their characteristic crystalline framework shows instability. In this article we characterise the structure and electrochemical behavior of manganese hexacyanochromate which exhibits reversible sodium insertion at −0.86 V vs. SHE (1.84 V vs. Na^+/Na), whilst maintaining the characteristic PBA cubic structure. This is the lowest redox potential of reported PBA materials and shows fast kinetics in a high voltage water-in-salt electrolyte. Further reduction in potential in an organic electrolyte shows decomposition of the crystalline structure.

Introduction

Prussian blue analogues (PBAs) are uniquely suitable as electrode materials for sodium ion (NIBs) and potassium ion batteries (KIBs) due to their open-framework structure, two possible redox centres, and compositional tunability[1,2]. Wide <100> ion conduction channels enable rapid solid-state diffusion of insertion ions. Large interstitial sites, larger than the insertion ion, and the robust framework result in minimal structural modification on ion insertion[3](Figure 1a). They have been explored for many different applications because of their ease of synthesis and intriguing electrochemical and magnetic properties[2].

Recently, we and others have utilized PBAs as battery materials with excellent cycle life and rate performance in both aqueous and organic electrolytes for NIBs and KIB[4–6]. Most of the previous work has been dedicated to the electrochemistry of hexacyanoferrates, where the C-coordinated Fe reversibly varies its oxidation state between III and II at potentials around 0.8 V vs. SHE (3.5 V vs. Na^+/Na), depending on the inductive effect of the N-coordinated transition metal ion, making them ideal positive electrode materials. The excellent properties of PBA cathode materials can only be fully exploited when combined in a full cell with an anode of comparable performance. This, and the lack of high performing sodium ion anode materials, motivate the search for PBA compositions that operate at lower potentials.

We have previously shown how replacing the C-coordinated Fe with Mn lowers the insertion potential to about 0 V vs. SHE ($Mn^{II}-N\equiv C-Mn^{III/II}$), approaching but within the thermodynamic stability limit of water[7–9]. Coupled with a copper hexacyanoferrate ($Cu^{II}-N\equiv C-Fe^{III/II}$) cathode an aqueous full cell with high performance and an

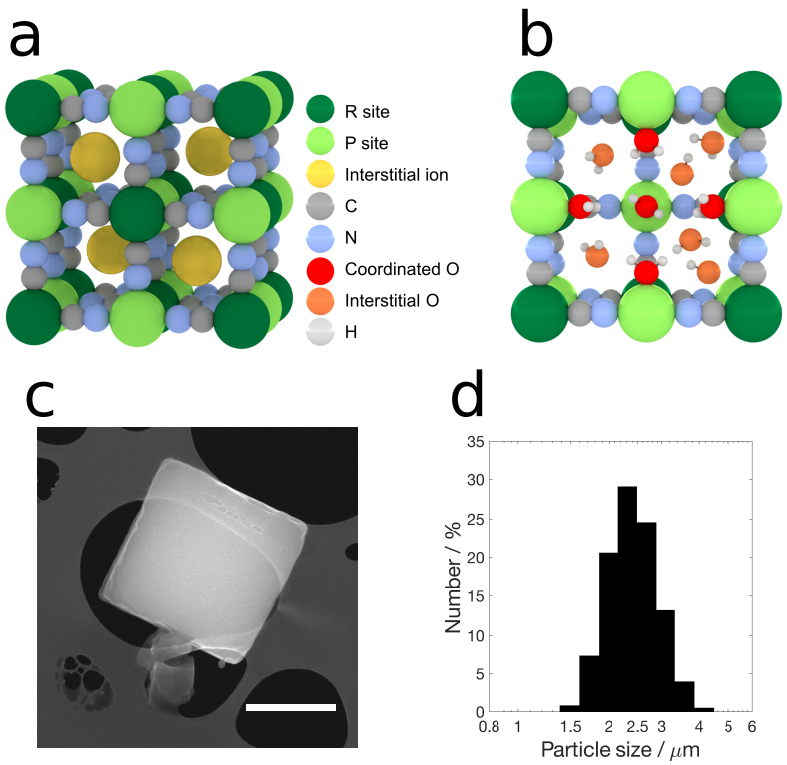

Figure 1: Schematic representation of cubic PBAs and morphology of MnHCCr. (a) the ideal PBA crystal structure consisting of two distinct transition metal sites, P and R, denoted by light green and dark green spheres respectively. These transition metals are octahedrally coordinated to cyanide ligands forming the cubic structure. Grey and light blue spheres are carbon and nitrogen. Within the structure there are interstitial sites which can accommodate inserting ions, shown in yellow. (b) Hexacyanometallate vacancies, $[R(CN)_6]$, are a major structural defect often up to 33 % in PBA materials, and water is present in the structure in two distinct bonding environments. (c) Scanning electron micrograph of as-synthesised MnHCCr, scale bar 1 µm. (d) Particle size distribution measured from dynamic light scattering (DLS) measurements.

average discharge potential of 1 V was produced[7]. Manganese hexacyanomanganate also has a lower redox couple at −0.7 V vs. SHE (Mn^{II}−N≡C−$Mn^{II/I}$)[8]. In order to access this redox couple whilst operating in an organic electrolyte a synthetic procedure to produce very low vacancy (1 %) and water content was developed. More recently this same redox couple was used with high vacancy (19 %) manganese hexacyanomanganate and operated in a water-acetonitrile co-solvent electrolyte[9].

There have been efforts to develop PBA materials that have active redox couples at more negative potentials, however attempts to date have resulted in loss of the crystal structure and high reversible capacities ascribable to conversion-type mechanisms[10,11]. These works highlight issues that arise when operating PBAs at low potentials in non-aqueous electrolytes but offer no explanation of the cause of structural breakdown.

By replacing the C-coordinated ion with Cr we can further reduce the redox potential[12]. In this work we characterise and investigate the redox behaviour of manganese hexacyanochromate (Mn^{II}−N≡C−$Cr^{III/II}$, referred to as MnHCCr in this paper) in a high voltage aqueous electrolyte. To the best of our knowledge, at −0.86 V vs. SHE it has a lowest redox potential of all PBA compounds where the reversible ion

insertion and structural integrity is confirmed. Further reduction in the potential within an organic electrolyte shows large irreversible capacity and a breakdown of the crystalline structure.

Results and Discussion

Manganese hexacyanochromate: physico-chemical characterization

MnHCCr was synthesised directly from $Mn(NO_3)_2$, $CrCl_3$ and NaCN in a one-pot two-step process (details in the Methods section). The as-synthesised powder has large cubic particles (Figure 1c), with an average particle size of around 2.3 µm. Inductively coupled plasma optical emission spectrometry (ICP-OES) and thermogravimetric analysis (TGA) were used to calculate chemical composition and water content respectively. The overall chemical formula was $Na_{0.04}Mn[Cr(CN)_6]_{0.70} \cdot 2.80\,H_2O$. Manganese coordination environment is therefore approximately MnN_4O_2, the remaining water within a hydration shell around sodium ions and hydrogen bonded within interstitial sites.

Prussian blue analogues often crystallize in the cubic space group Fm-3m. The structure contains two distinct transition metal sites, R and P, which are in an FCC arrangement and bridged by cyanide ligands. MnHCCr takes this crystal structure, with Mn and Cr sitting at 4a and 4b sites respectively, whilst C and N taking 24e sites (x, 0, 0)[13]. Sodium sits at the centre of the interstitial site (8c). Water is present in the structure in two distinct bonding environments: co-ordinated water bonded directly to P-site transition metals within vacancies and zeolitic water which are distributed loosely-bound throughout the structure[13,14].

High-resolution synchrotron powder diffraction data was taken of the hydrated MnHCCr which was used for structural refinement (Figure 2).

Sodium was removed from the model due to its low occupancy, 0.04 per formula unit from ICP. Two oxygen sites were included in the model, O(1) at 8c in the centre of the interstitial site and O(2) at 24e bonded to manganese in vacancies. In the model oxygen atoms represent water molecules, with hydrogen atoms removed due to their extremely low scattering. Similar treatment of water molecules in PBAs have been undertaken previously[13,15,16]. Figure 2 shows the high-resolution XRD data with Rietveld fitting and residual. The large particle size and high crystallinity result in high-intensity well-defined peaks, even at high angles. Final refinement parameters are given in Table 1.

The lattice parameter is calculated to be 10.804 Å, within the range of previously reported values[13,17,18]. Lattice parameter is highly sensitive to level of hydration with accounts for the relatively wide range of values in literature. The hexacyanochromate vacancy content was calculated to be 31 %, in good agreement with ICP results of 30 %. The total water content was higher than that calculated from TGA. This is likely due to an underestimation of the water content calculated from the mass loss in TGA due to dehydration before the measurement starting.

The two oxygen positions are reasonable and supported by TGA and FTIR data (Figure 3). The refinement gave an occupancy of 0.41 for O(2) coordinated water, close to the expected value of 0.3. High atomic displacement parameter for the zeolitic water, O(1), indicate that there are imperfections in the model. The high vacancy content and lack of apparent ordering of the vacancies throughout the structure results in a number of local environments within the structure. In theory each interstitial site can be adjacent to zero, one, two, three or four hexacyanochromate vacancies. This in turn leads to a number of oxygen sites both at the centre of the interstitial site (8c) and displaced along the <111> directions (32f) and <110> directions (48g)[15]. Additionally, hydrogen bonding to co-ordinated water can result in lower energy positions off-centre[13,14]. This multitude of factors result in a particularly complex arrangement of water molecules within interstitial sites and efforts to further refine O(1) oxygen sites proved unsuccessful.

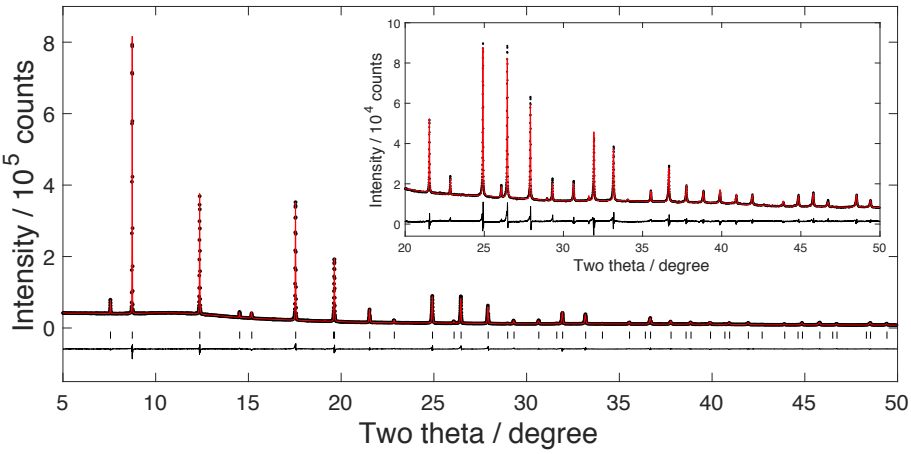

Figure 2: High-resolution synchrotron powder X-ray diffraction pattern of as-synthesised hydrated MnHCCr ($\lambda = 0.824\,525$ Å).

Atom	Site	g	x	y	z	U_{iso}
Mn	4a	1	0	0	0	0.028
Cr	4b	0.693	0.5	0	0	0.023
O(1)	8c	1.422	0.25	0.25	0.25	0.403
C	24e	0.693	0.308	0	0	0.065
N	24e	0.693	0.200	0	0	0.034
O(2)	24e	0.412	0.245	0	0	0.191

Table 1: Structural parameters of MnHCCr from Rietveld refinement in the space group Fm-3m (Z = 4). Occupancy g, atomic positions (x, y, z), and isotropic atomic displacement U_{iso} are given. The lattice parameter is 10.804 Å. Sodium is located at the centre of the interstitial A site whilst oxygen takes two positions, O(1) bonded to Mn in vacancies and O(2) at the centre of the interstitial site. $R_P = 1.65\%$, $R_{WP} = 2.79\%$, $\chi^2 = 16.26$, GOF = 4.03.

Effect of water on structural stability

Thermal analysis was performed through simultaneous thermal gravimetric analysis, differential scanning calorimetry and mass spectrometry, Figure 3a.

Between 30 °C and 150 °C there is the first mass loss step, corresponding to dehydration of the materials as seen through the m/z=18 mass spectrometry trace. Within this trace there are two distinct water evolutions steps which could correspond to water loss from two distinct environments, firstly the loosely bound zeolitic water and the second the coordinated water molecules at higher temperatures. This is most clearly seen in the DSC trace as two distinguishable endothermic steps peaking at 80 °C and 124 °C. The second mass loss step shows CO_2 release which is indictive of breakdown of the crystalline structure.

In attempt to study the material at different levels of hydration samples were dried at RT, 80 °C, 150 °C and 220 °C under vacuum. The FTIR spectra and XRD patterns these samples are shown in Figure 3b and c. The characteristic stretching band of CN is the most intense peak and at 2164 cm^{-1} in the most hydrated sample, increasing to 2166 cm^{-1} then 2170 cm^{-1} as water is removed. This is consistent with previous reports[19]. The broad band between 3100 cm^{-1} to 3700 cm^{-1} as well as the sharp peaks at 3604 cm^{-1} and 3650 cm^{-1} come from stretching modes of water in the sample. The strong

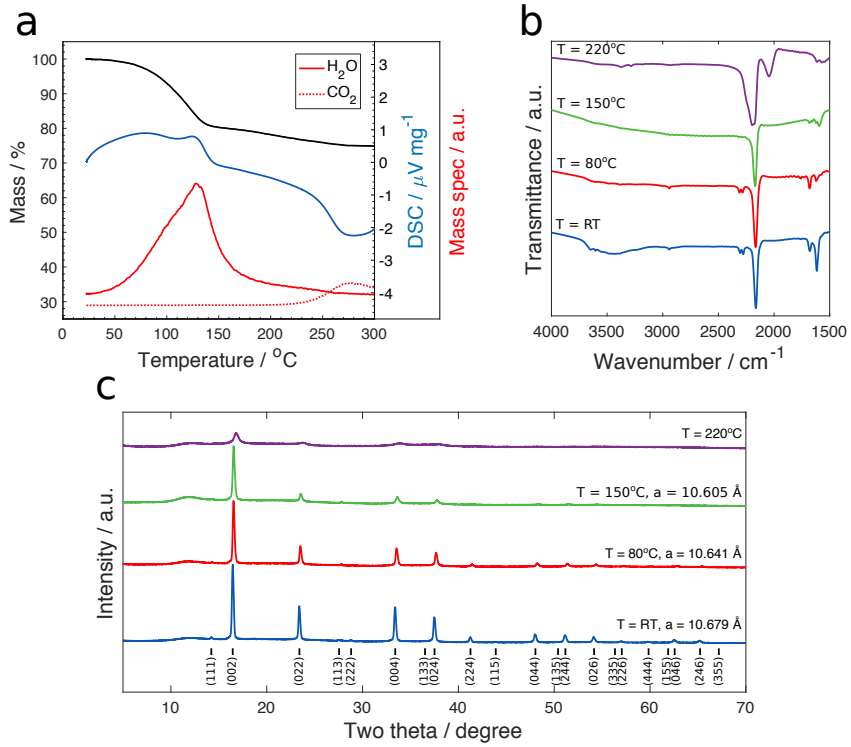

Figure 3: Dehydration of MnHCCr. The composition, bonding, and structure of MnHCCr was explored after heating at a series of temperatures. (a) The thermal gravimetric analysis (TGA) trace of as synthesised MnHCCr shows two distinct mass lost steps, the first accounting for 20 % of initial mass, the second accounting for 5 %. Simultaneous differential scanning calorimetry (DSC) shows distinct endothermic and exothermic processes. Mass spectrometry shows the first step is the dehydration of the material, followed by carbon dioxide evolution at higher temperature. (b) FTIR shows bonding within the samples. The stretching mode of CN, the most intense peak, is seen at 2164 cm^{-1}. Different stretching and bending modes of water are responsible for absorption bands between 1600 cm^{-1} to 1700 cm^{-1} and 3100 cm^{-1} to 3700 cm^{-1}. (c) the dependence of structure on heating temperature is shown in XRD data.

broad peak corresponds to hydrogen bonded water molecules with rotational freedom. Heating to 80 °C removes this absorption band. Sharp bands at 3604 cm^{-1} and 3650 cm^{-1} correspond to the symmetric and asymmetric stretching modes of coordinated water. Sharp absorption bands in the range 1600 cm^{-1} to 1700 cm^{-1} correspond to bending modes of water. In the hydrated sample two peaks are seen at 1616 cm^{-1} and 1678 cm^{-1}. On dehydration at 80 °C the peak at 1616 cm^{-1} reduces in intensity considerably whereas the peak at 1678 cm^{-1} does not change. This leads to the conclusion that the less strongly bound zeolitic water is responsible for the peak at 1616 cm^{-1} and coordinated water is responsible for the peak at 1678 cm^{-1} [20]. Peaks in the IR spectra between 2260 cm^{-1} and 2320 cm^{-1} and at 2945 cm^{-1} are from acetonitrile impurities introduced during the washing procedure.

XRD patterns of the same samples show a decrease in lattice parameter as the materials is dehydrated and a loss in the crystalline structure at 220 °C. Additionally, as the material is dehydrated the relative intensities of high angle reflections decrease considerably which is likely due to local structural distortion and increased microstrain. High-resolution synchrotron powder X-ray diffraction of MnHCCr dried at 80 °C under vacuum is shown in Supplementary Fig-

ure 1. Refinement parameters in Supplementary Table 1 show a larger decrease in interstitial water removal compared to coordinated water, further supporting the TGA-DSC-MS and FTIR data.

For electrochemical studies hydrated electrodes were used in the water-based electrolyte and electrodes dehydrated at 150 °C under vacuum where used in a non-aqueous electrolyte. This dehydration temperature was chosen because much, if not all, of the water was removed but the crystalline structure was still present.

Electrochemical characterization in a water-in-salt electrolyte

The electrochemical behaviour of MnHCCr was characterised in a water-containing electrolyte. Experimentally it has been shown that PBAs exhibit extremely fast electrode kinetics in aqueous electrolytes, especially when the material has high vacancy content[6,7]. This is reportedly due to very low interfacial charge transfer and high ionic mobility within the structure as water shields local charges[21]. Additionally, DFT modelling has shown a stabilizing effect of structural water in PBA materials[22]. Since MnHCCr has such a low redox potential, much lower than the thermodynamic limit of water, the use of conventional aqueous electrolytes is prohibited.

In this study an aqueous water-in-salt (WiS) sodium bis(fluorosulfonyl)imide (NaFSI) electrolyte at 37 m was used (prepared according to ref[23]). This is a new class of electrolytes for which the electrochemical stability window is significantly increased through reduced activity of water, strong bonding between water molecules and cations in solution, and potentially the formation of a Na^+ conducting solid-electrolyte interphase[23,24]. This electrolyte was used as it has one of the widest electrochemical stability windows of electrolytes that contain water.

The electrochemical stability window of this electrolyte was measured by LSV experiments on glassy carbon electrode at $1\,\mathrm{mV\,s^{-1}}$ (Figure 4a).

Using a current density limit of $10\,\mu\mathrm{A\,cm^{-2}}$ the electrolyte has a lower stability limit of 1.07 V vs. SHE and a stability window of 2.5 V. MnHCCr shows a reversible electrochemical reaction centred at −0.86 V vs. SHE, the dQ/dV of this reaction is shown in Figure 4a alongside $MnHCFe^{III/II}$ for comparison. MnHCCr gave a reversible capacity of $62\,\mathrm{mA\,h\,g^{-1}}$ which is expected from a single redox centre PBA material with vacancy content of 30 %. A full PBA cell could be produced by coupling this with MnHCFe or any other PBA cathode material[25].

Cyclic voltammograms at scan rates from $0.1\,\mathrm{mV\,s^{-1}}$ to $10\,\mathrm{mV\,s^{-1}}$ were performed to study the redox reaction kinetics (Figure 4b). As the scan rate increases the peak separation increases and the peak current increases linearly with the root of scan rate. This behaviour is indicative of a one-electron one-step quasi reversible reaction within a diffusion limited regime.

For such systems the dependence of peak current, $\mathrm{i_{rate}}$ (mA) , on scan rate is given by[26]

$$i_{rate} = 0.4463 \cdot \sqrt{\frac{n^3 F^3}{RT}} \cdot \sqrt{D} \cdot C_o \cdot \sqrt{V_{rate}}$$

where n is the number of electrons involved in the reaction, D ($\mathrm{cm\,s^{-1}}$) is the average diffusion coefficient, $\mathrm{C_0}$ ($\mathrm{mol\,cm^{-3}}$) is the concentration of active sites, $\mathrm{V_{rate}}$ ($\mathrm{mV\,s^{-1}}$) is the scan rate and F, R, and T take their conventional meanings. $\mathrm{C_0}$ can be estimated from the specific capacity and density of the material. Using the gradient of the line of best fit during oxidation of $1.07\,\mathrm{mA\,s^{1/2}\,V^{-1/2}}$, Figure 4c, gives an average diffusion coefficient of $1.9 \times 10^{-6}\,\mathrm{cm^2\,s^{-1}}$. This value is high for solid state diffusion and similar in order of magnitude to diffusion in other PBA compounds[27].

To study the electrode reaction MnHCCr electrodes were cycled twice and then on the third discharge stopped at various states of charge. Ex situ XRD patterns show that the structure remained cubic and Figure 5a shows the two-theta angle of the (024) peaks.

Refinement of the unit cell shows that the lattice parameter changes linearly with the state of charge over the whole range (Figure 5b). As the material is reduced, and sodium inserted into the material, the lattice parameter decreases. This peculiar behaviour is seen in other PBA materials and the change in lattice parameter is caused by the change in the $\mathrm{Cr(CN)_6^{n-}}$ complex radius as it alters valence state[28,29]. The

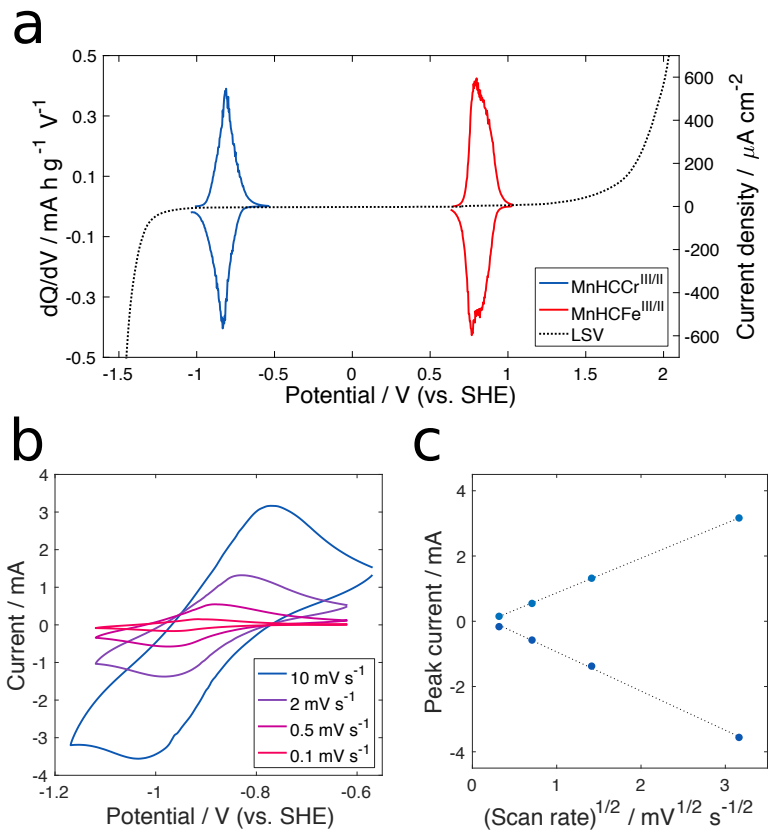

Figure 4: MnHCCr aqueous electrochemical characterisation. (a) linear sweep voltammetry (LSV) of the water-in-salt (WiS) electrolyte was taken using a glassy carbon pin at $1\,\mathrm{mV\,s^{-1}}$, with the electrochemical stability limit defined as $10\,\mu\mathrm{A\,s^{-2}}$. The dQ/dV of $Mn^{II}-N{\equiv}C-Cr^{III/II}$ and $Mn^{II}-N{\equiv}C-Fe^{III/II}$ are shown, centered at $-0.86\,\mathrm{V}$ vs. SHE and $0.80\,\mathrm{V}$ vs. SHE respectively. (b) cyclic voltammograms (CVs) of MnHCCr at scan rates from $0.1\,\mathrm{mV\,s^{-1}}$ to $10\,\mathrm{mV\,s^{-1}}$. (c) the peak current at each scan rate plotted against the square root of scan rate. The gradients of the lines of best fit are $1.07\,\mathrm{mA\,s^{1/2}\,V^{-1/2}}$ and $-1.20\,\mathrm{mA\,s^{1/2}\,V^{-1/2}}$.

material exhibits a very low lattice parameter variation of 0.6 % on cycling.

The position of the ν(CN) band is dependent on the bonding environment, and in the case of MnHCCr the oxidation state of Mn and Cr, which is analogous to other PBA materials[7,15,30]. Ex situ FTIR shows that as the material is reduced there is a decrease in the absorption peak at $2164\,\mathrm{cm^{-1}}$, characteristic of $Mn^{II}-N{\equiv}C-Cr^{III}$ bonding, and an increase in the peak at $2049\,\mathrm{cm^{-1}}$, characteristic of $Mn^{II}-N{\equiv}C-Cr^{II}$ bonding, Figure 5c. Both the change in lattice parameter and FTIR spectra were observed to be fully reversible.

Further reduction in potential in an organic electrolyte

To explore the stability of the material at lower potentials the electrochemical behavior of the material was explored in an organic electrolyte (1 M $NaClO_4$ in PC). The electrodes were dried under vacuum at 150 °C to remove water within the structure before use. Figure 6 shows the galvanostatic cycling performance, at $15\,\mathrm{mA\,g^{-1}}$, of MnHCCr in WiS and in organic electrolyte with two different cut-off voltages. Additionally, ex situ XRD were taken at selected points. Operating in an organic electrolyte with the voltage cut-off at $-1.3\,\mathrm{V}$ MnHCCr shows the single re-

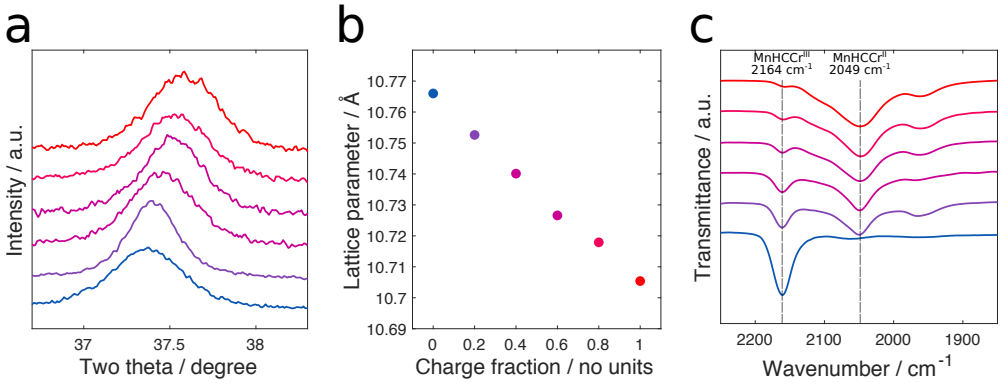

Figure 5: Ex-situ analysis of MnHCCr electrode reaction in an aqueous electrolyte. Ex-situ XRD at various charge states between 0 and 1.0 shows a linear contraction in the lattice on reduction, show in (a) by the (024) diffraction peak moving to higher angles. The cubic structure of MnHCCr is maintained over the whole state of charge. In addition to the change in lattice parameter the intensity of the (022) and (004) peaks increased, compared to the (002), as the material is reduced, and sodium inserted. (b) shows the dependence of state of charge on lattice parameter, calculated through refinement of the lattice parameter of a cubic unit cell. Ex-situ FTIR was performed on the same electrodes and shows the change in v(CN) absorption as the CN^- environment is changing. The absorption peak at 2164 cm^{-1} is characteristic of $Mn^{II}-N\equiv C-Cr^{III}$ bonding whereas the peak at 2049 cm^{-1} is characteristic of $Mn^{II}-N\equiv C-Cr^{II}$ bonding.

versible plateau corresponding to the reduction of chromium, as seen in the WIS electrolyte previously. Ex situ XRD confirms the structure is maintained. There is, however, lower capacity and slower kinetics when compared to performance in the WiS electrolyte. The Na+ diffusion coefficient of dehydrated MnHCCr was calculated to be $3 \times 10^{-8}\,cm^2\,s^{-1}$, more than an order of magnitude lower than the hydrated material, see Supplementary Figure 2.

With a cut-off voltage at −1.65 V there is an additional voltage plateau centered at −1.45 V. This plateau has a large irreversible capacity and corresponds to the permanent breakdown of the crystalline structure. This is a similar response to other PBA compositions that have been discharged to low potentials in non-aqueous electrolytes and where reversible capacity arises from conversion-type mechanisms[10,11]. Finding the limit of stability of the MnHCCr crystalline structure, and of PBA compounds more generally, is significant and places fundamental limitations on the useable potential range of the material.

Conclusions

In summary, we characterise the structure and electrochemical behavior of manganese hexacyanochromate which exhibits reversible sodium insertion at −0.86 V vs. SHE, whilst maintaining the characteristic open-framework PBA structure. The material has a capacity of 62 $mA\,h\,g^{-1}$ and a diffusion coefficient of $1.9 \times 10^{-6}\,cm^2\,s^{-1}$ whilst operating in a high voltage water-in-salt electrolyte. This capacity is a result of the one-electron reaction and the high hexacyanochromate vacancy content of 30 %. These vacancies are positive defects which decrease the sodium content stored in the material when reduced, and so decrease the available capacity. Ex situ XRD has shown that the materials exhibits very low strain, of less than 1 %, on cycling.

MnHCCr has the lowest redox potential for which the preservation of the open-framework structure is confirmed, and charge storage is from sodium insertion and transition metal redox. This is important as the limit of stability of PBA materials at low potential is currently unknown. When investigating the material in

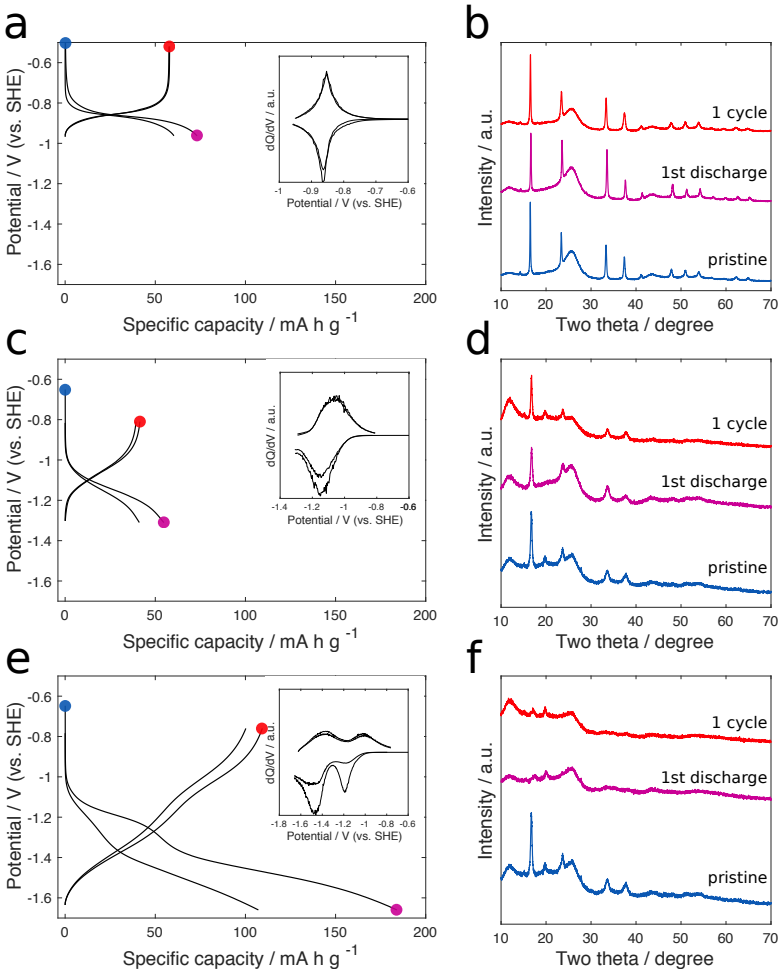

Figure 6: Behavior of MnHCCr during the first two cycles in the WiS electrolyte (a) and in an organic electrolyte with different voltage cut-offs (c and e). XRD patterns of ex situ samples are shown, taken in the pristine state, after one discharge and after one full discharge and charge cycle for each cycling conditions (b, d and f). Note samples cycled in the organic electrolyte were dried at 150 °C under vacuum. Peaks in the XRD patterns at 18.3°, 19.8° and 27.8° come from the PVDF binder, see Supplementary Figure 3.

an organic electrolyte the same redox couple is observed, and the diffusion coefficient was calculated to be more than an order of magnitude lower at $3 \times 10^{-8}\,\mathrm{cm^2\,s^{-1}}$. Reducing the potential lower than $-1.3\,\mathrm{V}$ vs. SHE resulted in irreversible loss in the crystal structure and a change in the charge storage mechanism.

This work deepens the understanding of the limits of stability of the materials system and the relationship between vacancy and water content to performance and stability. Further research should be focused on overcoming the partial solubility of PBA compounds in aqueous electrolytes that, currently, leads to poor cycle life.

Experimental Methods

Manganese hexacyanochromate synthesis

5 g of NaCN and 3 g of $CrCl_3$ (excess $CrCl_3$) were added to 120 ml of 0.1 M HCl solution. The

solution was refluxed for 30 min. Then 4.819 g of 47.5 % $Mn(NO_3)_2$ solution was added under stirring in a dropwise manner. After 30 min the precipitate was centrifuged, washed three times with DI water and once with acetonitrile then dried overnight at 80 °C in air.

Manganese hexacyanoferrate synthesis

0.5 M $Na_4Fe(CN)_6$ solution was added in a dropwise manner to 1.5 M $Mn(NO_3)_2$ solution under stirring at 30 °C such that the final solution had a stoichiometric ratio of Fe to Mn. Both initial solutions contained 4 M NaCl. The solution was left to stir for 30 min then the precipitate was centrifuged, washed three times with DI water and once with acetonitrile then dried overnight at 80 °C in air.

Materials characterization

Elemental composition was determined by inductively coupled plasma optical emission spectrometry (Perkin Elmer Optima 8000) and thermal analysis was performed using simultaneous thermogravimetric analysis mass spectrometry (NETZSCH STA 449 F3 Jupiter coupled to a QMS 403 Aolos). Microscopy was carried out on a FE-SEM (Zeiss Merlin). Synchrotron X-ray diffraction was performed at beamline i11 at Diamond Light Source on the position sensitive detector (PSD). XRD of dehydrated MnHCCr samples and ex situ electrodes were performed inside a N_2 filled glove box (Rigaku MiniFlex Cu source). Fourier transform infrared spectroscopy (Thermo Scientific Nicolet 6700) was performed in transmission mode using CsI pellets within a nitrogen filled glove box. Ex situ samples for XRD and FTIR were prepared by retrieving the carbon cloth electrodes, washing them with acetonitrile, then allowing them to dry before measurement. For FTIR samples the powder was then scraped from the carbon cloth. The General Structure Analysis System/Experiment Graphical User Interface (GSAS/EXPGUI) program was used for refinements[31,32]. The particle-size distribution was measured using dynamic light scattering (Malvern Zetasizer Nano ZS) using a He-Ne laser (633 nm). The sample was prepared by dispersing the powder in a 1:1 mixture of water/isopropanol through sonication.

Electrochemical characterization

Electrodes were prepared by mixing 80 wt % active material, 10 wt % carbon black (Timical SUPER C65) and 10 wt % polyvinylidene fluoride (Kynar 2850 GL) in a mortar with 1-methyl-2- pyrrolidone to form a slurry. The slurry was pasted on carbon cloth (Fuel Cell Earth AvCarb) with areal mass loadings of around 10 mg cm^{-2}, then dried overnight at 80 °C in air. Electrochemical measurements were performed on three electrode flooded cells inside an Ar filled glove box. For aqueous measurements the reference electrode was an Ag/AgCl pseudo reference prepared through oxidation of silver wire in HCl solution which was calibrated using a ferrocene internal standard. The counter electrode was MnHCFe. For non-aqueous measurements sodium metal was used as both reference and counter electrodes. Electrochemical measurements were performed on a BioLogic VMP3 potentiostat.

Acknowledgements

This publication arises from research funded by the John Fell Oxford University Press Research Fund. S.W. acknowledges financial support from EPSRC. We thank Diamond Light Source for access to beamline I11 (proposal number EE14809-1) that contributed to the results presented here.

Author contributions

S.W. and M.P designed electrochemical and physical measurements. S.W. and I.C., performed and analyzed electrochemical measurements and physical characterization. S.W., S.D., C.T. and M.P. designed and performed the synchrotron X-ray diffraction measurements. S.W. and M.P. wrote this paper.

Competing interest

The authors declare no competing financial interests.

References

[1] K. Hurlbutt, S. Wheeler, I. Capone, and M. Pasta, "Prussian Blue Analogs as Battery Materials," *Joule*, vol. 2, pp. 1950–1960, aug 2018.

[2] J. Qian, C. Wu, Y. Cao, Z. Ma, Y. Huang, and X. Ai, "Prussian Blue Cathode Materials for Sodium-Ion Batteries and Other Ion Batteries," *Advanced Energy Materials*, vol. 1702619, pp. 1–24, 2018.

[3] C. D. Wessells, S. V. Peddada, R. A. Huggins, and Y. Cui, "Nickel Hexacyanoferrate Nanoparticle Electrodes For Aqueous Sodium and Potassium Ion Batteries," *Nano Letters*, vol. 11, pp. 5421–5425, 2011.

[4] M. Pasta, R. Y. Wang, R. Ruffo, R. Qiao, H. W. Lee, B. Shyam, M. Guo, Y. Wang, L. A. Wray, W. Yang, M. F. Toney, and Y. Cui, "Manganese-cobalt hexacyanoferrate cathodes for sodium-ion batteries," *Journal of Materials Chemistry A*, vol. 4, no. 11, pp. 4211–4223, 2016.

[5] L. Wang, J. Song, R. Qiao, L. A. Wray, M. A. Hossain, Y. D. Chuang, W. Yang, Y. Lu, D. Evans, J. J. Lee, S. Vail, X. Zhao, M. Nishijima, S. Kakimoto, and J. B. Goodenough, "Rhombohedral Prussian white as cathode for rechargeable sodium-ion batteries," *Journal of the American Chemical Society*, vol. 137, no. 7, pp. 2548–2554, 2015.

[6] C. D. Wessells, R. a. Huggins, and Y. Cui, "Copper hexacyanoferrate battery electrodes with long cycle life and high power.," *Nature communications*, vol. 2, p. 550, 2011.

[7] M. Pasta, C. D. Wessells, N. Liu, J. Nelson, M. T. McDowell, R. A. Huggins, M. F. Toney, and Y. Cui, "Full open-framework batteries for stationary energy storage," *Nature Communications*, vol. 5, p. 3007, jan 2014.

[8] H.-W. Lee, R. Y. Wang, M. Pasta, S. Woo Lee, N. Liu, and Y. Cui, "Manganese hexacyanomanganate open framework as a high-capacity positive electrode material for sodium-ion batteries," *Nature communications*, vol. 5, p. 5280, oct 2014.

[9] A. Firouzi, R. Qiao, S. Motallebi, C. W. Valencia, H. S. Israel, M. Fujimoto, L. A. Wray, Y. D. Chuang, W. Yang, and C. D. Wessells, "Monovalent manganese based anodes and co-solvent electrolyte for stable low-cost high-rate sodium-ion batteries," *Nature Communications*, vol. 9, no. 1, 2018.

[10] P. Nie, L. Shen, H. Luo, B. Ding, G. Xu, J. Wang, and X. Zhang, "Prussian blue analogues: a new class of anode materials for lithium ion batteries," *J. Mater. Chem. A*, vol. 2, no. 16, pp. 5852–5857, 2014.

[11] T. Shibata, M. Takachi, and Y. Moritomo, "Low Voltage Charge/Discharge Behavior of Manganese Hexacyanoferrate," *Batteries*, vol. 3, no. 1, p. 7, 2017.

[12] F. Scholz and A. Dostal, "The Formal Potentials of Solid Metal Hexacyanometalates," *Angewandte Chemie International Edition in English*, vol. 34, pp. 2685–2687, jan 1996.

[13] H. U. Güdel, H. Stucki, and A. Ludi, "The crystal structure of manganese(II) hexacyanochromate(III), Mn3[Cr(CN)6]2·xH2O," *Inorganica Chimica Acta*, vol. 7, no. C, pp. 121–124, 1973.

[14] F. Herren, A. Ludi, P. Fischer, and W. Halg, "Neutron Diffraction Study of Prussian Blue, Fe4[Fe(CN)6]3.xH2O. Location of Water Molecules and Long-Range Magnetic Order," *Inorganic Chemistry*, vol. 19, no. 4, pp. 956–959, 1980.

[15] D. O. Ojwang, J. Grins, D. Wardecki, M. Valvo, V. Renman, L. Häggström, T. Ericsson, T. Gustafsson, A. Mahmoud,

R. P. Hermann, and G. Svensson, "Structure Characterization and Properties of K-Containing Copper Hexacyanoferrate," *Inorganic Chemistry*, vol. 55, no. 12, pp. 5924–5934, 2016.

[16] R. Y. Wang, B. Shyam, K. H. Stone, J. N. Weker, M. Pasta, H. W. Lee, M. F. Toney, and Y. Cui, "Reversible Multivalent (Monovalent, Divalent, Trivalent) Ion Insertion in Open Framework Materials," *Advanced Energy Materials*, vol. 5, no. 12, pp. 1–10, 2015.

[17] W. Dong, L. N. Zhu, H. B. Song, D. Z. Liao, Z. H. Jiang, S. P. Yan, P. Cheng, and S. Gao, "A Prussian-Blue Type Ferrimagnet Na[MnCr(CN)6]: Single Crystal Structure and Magnetic Properties," *Inorganic Chemistry*, vol. 43, no. 8, pp. 2465–2467, 2004.

[18] A. Ferrari, M. E. Tani, and E. Morisi, "The crystal structure of hexacyanochromate(III) of divalent cations," *Acta Crystallographica*, vol. 15, no. 1, pp. 90–90, 1962.

[19] D. B. Brown and D. F. Shriver, "Structures and solid-state reactions of prussian blue analogs containing chromium, manganese, iron, and cobalt," *Inorganic Chemistry*, vol. 8, no. 1, pp. 37–42, 1969.

[20] M. Avila, L. Reguera, J. Rodríguez-Hernández, J. Balmaseda, and E. Reguera, "Porous framework of T2[Fe(CN)6]·xH2O with T=Co, Ni, Cu, Zn, and H2 storage," *Journal of Solid State Chemistry*, vol. 181, no. 11, pp. 2899–2907, 2008.

[21] Y. Mizuno, M. Okubo, E. Hosono, T. Kudo, H. Zhou, and K. Oh-Ishi, "Suppressed activation energy for interfacial charge transfer of a Prussian blue analog thin film electrode with hydrated ions (Li+, Na +, and Mg2+)," *Journal of Physical Chemistry C*, vol. 117, no. 21, pp. 10877–10882, 2013.

[22] P. Xiao, J. Song, L. Wang, J. B. Goodenough, and G. Henkelman, "Theoretical study of the structural evolution of a Na2FeMn(CN)6cathode upon Na intercalation," *Chemistry of Materials*, vol. 27, no. 10, pp. 3763–3768, 2015.

[23] R.-S. Kühnel, D. Reber, and C. Battaglia, "A High-Voltage Aqueous Electrolyte for Sodium-Ion Batteries," *ACS Energy Letters*, pp. 2005–2006, 2017.

[24] L. Suo, O. Borodin, Y. Wang, X. Rong, W. Sun, X. Fan, S. Xu, M. A. Schroeder, A. V. Cresce, F. Wang, C. Yang, Y. S. Hu, K. Xu, and C. Wang, "Water-in-Salt Electrolyte Makes Aqueous Sodium-Ion Battery Safe, Green, and Long-Lasting," *Advanced Energy Materials*, vol. 7, no. 21, pp. 1–10, 2017.

[25] K. Nakamoto, R. Sakamoto, Y. Sawada, M. Ito, and S. Okada, "Over 2 V Aqueous Sodium-Ion Battery with Prussian Blue-Type Electrodes," *Small Methods*, vol. 1800220, p. 1800220, 2018.

[26] A. J. Bard and L. R. Faulkner, *Electrochemical methods: fundamentals and applications*. 1980.

[27] H.-W. Lee, M. Pasta, R. Y. Wang, R. Ruffo, and Y. Cui, "Effect of the alkali insertion ion on the electrochemical properties of nickel hexacyanoferrate electrodes," *Faraday Discuss.*, vol. 176, pp. 69–81, 2014.

[28] R. J. Deeth, "A theoretical rationale for the formation, structure and spin state of pentacyanochromate(II)," *European Journal of Inorganic Chemistry*, no. 13, pp. 2551–2555, 2006.

[29] M. Takachi, T. Matsuda, and Y. Moritomo, "Cobalt hexacyanoferrate as cathode material for na+ secondary battery," *Applied Physics Express*, vol. 6, no. 2, 2013.

[30] S. J. Gerber and E. Erasmus, "Electronic effects of metal hexacyanoferrates: An XPS and FTIR study," *Materials Chemistry and Physics*, vol. 203, pp. 73–81, 2018.

[31] R. B. Von Dreele and A. C. Larson, "General Structure Analysis Sytem (GSAS)," *Los Alamos National Lab*, vol. LAUR, pp. 86–748, 1994.

[32] B. H. Toby, "EXPGUI a graphical user interface for GSAS," *J. Appl. Cryst*, vol. 34, pp. 210–213, 2001.

Low Potential Prussian Blue Analogs: Manganese Hexacyanochromate

Samuel Wheeler[1], Isaac Capone[1], Sarah Day[2], Chiu Tang[2], Mauro Pasta[1,*]

[1]Department of Materials, University of Oxford, Parks Road, Oxford OX1 3PH, United Kingdom

[2]I11 Beamline, Diamond Light Source Limited, Harwell Science and Innovation Campus, Chilton, Didcot OX11 0DE, United Kingdom

*Correspondence: mauro.pasta@materials.ox.ac.uk

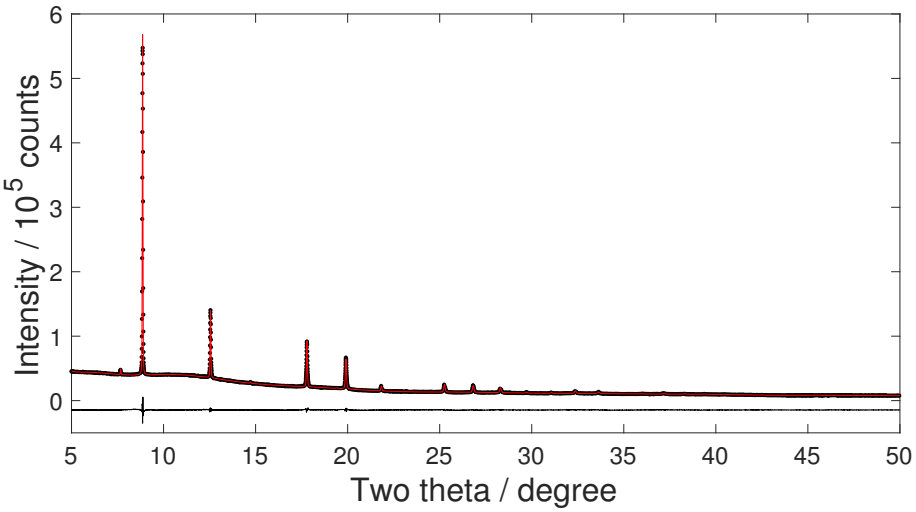

Supplementary Figure 1: High-resolution synchrotron powder X-ray diffraction pattern of MnHCCr dried at 80 °C under vacuum ((λ = 0.824 525 Å).

Atom	Site	g	x	y	z	U_{iso}
Mn	4a	1	0	0	0	0.028
Cr	4b	0.693	0.5	0	0	0.023
O(1)	8c	1.422	0.25	0.25	0.25	0.403
C	24e	0.693	0.308	0	0	0.065
N	24e	0.693	0.200	0	0	0.034
O(2)	24e	0.412	0.245	0	0	0.191

Supplementary Table 1: Structural parameters of MnHCCr dried at 80 °C under vacuum from Rietveld refinement in the space group Fm-3m (Z = 4). Occupancy g, atomic positions (x, y, z), and isotropic atomic displacement U_{iso} are given. The lattice parameter is 10.661 Å. Sodium is located at the centre of the interstitial A site whilst oxygen takes two positions, O(1) bonded to Mn in vacancies and O(2) at the centre of the interstitial site. R_P = 1.16%, R_{WP} = 1.58%, χ^2 = 4.797, GOF = 2.19.

Composition from SXRD refinement.
RT: $Mn[Cr(CN)_6]_{0.69} \cdot 2.84\,H_2O(1).2.47\,H_2O(2)$
80 °C under vacuum: $Mn[Cr(CN)_6]_{0.70} \cdot 0.69\,H_2O(1).1.46\,H_2O(2)$

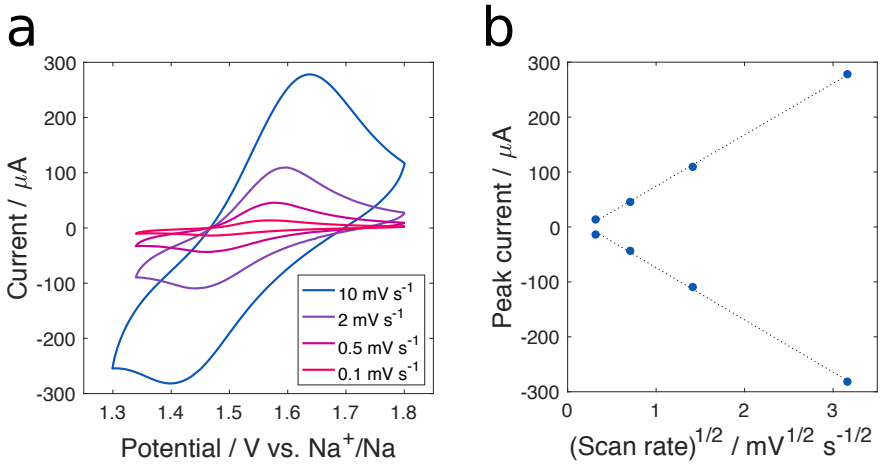

Supplementary Figure 2: Diffusion coefficient of Na^+ in dehydrated MnHCCr in an organic electrolyte (1 Molar in $NaClO_4$).

Average gradient of lines of best fit in Supplementary Figure 2b is $0.094\,mA\,s^{1/2}\,V^{-1/2}$. Diffusion coefficient was calculated to be $3 \times 10^{-6}\,cm^2\,s^{-1}$. This is approximately two orders of magnitude lower than the diffusion coefficient when hydrated in the WiS electrolyte.

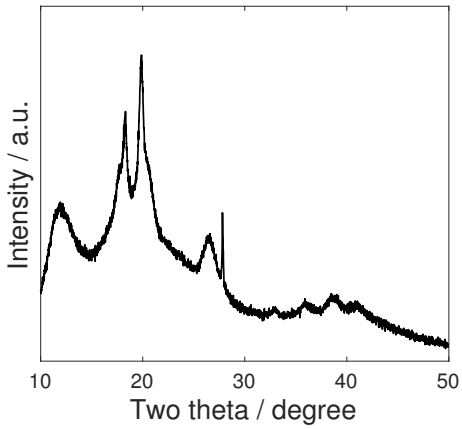

Supplementary Figure 3: X-ray diffractogram of PVDF binder.